

Article

Dynamics of Coalesced Droplet Jumping on Superhydrophobic Surface with Asymmetrically Wettable Ridge

Sungchan Yun 

Department of Mechanical Engineering, Korea National University of Transportation,
Chungju 27469, Republic of Korea; syun@ut.ac.kr

Abstract: Spontaneous detachment from superhydrophobic surfaces can be induced by the coalescence of two or more adjacent droplets. The phenomena have provided implications for the self-removal of droplets in the fields of self-cleaning, anti-icing, and heat transfer. However, many studies focus mainly on the theoretical jumping direction perpendicular to the substrate, although the velocity in the horizontal direction must be involved in practical applications due to various scenarios. This study analyzes numerically the effect of the distribution in ridge structure's wettability on the performance of coalesced droplet jumping. The jumping dynamics are discussed for varying contact angle ratios and the aspect ratios of the ridge, which are the initial values for the current model. We obtain the height of the jumping and the offset distance in the horizontal direction under the several initial values. In addition, the characteristics of the asymmetric behavior are discussed based on the temporal evolution of the average velocities of the jumping droplets for each direction. Numerical results show that the horizontal offset distance is significantly pronounced at both the high asymmetry in wettability and the high aspect ratio of the ridge geometry. The phenomenon occurs when the droplet detaches from the ridge surface in the retraction process. We determine the role of the distribution within the ridge structure on its wettability, as well as the role of the aspect ratios of the ridge in facilitating the efficient transport of droplets.

Keywords: superhydrophobic surface; interfacial dynamics; coalescence jumping; self-cleaning



Citation: Yun, S. Dynamics of Coalesced Droplet Jumping on Superhydrophobic Surface with Asymmetrically Wettable Ridge. *Appl. Sci.* **2024**, *14*, 3584. <https://doi.org/10.3390/app14093584>

Academic Editors: Ricardo Castedo

Received: 26 February 2024

Revised: 2 April 2024

Accepted: 17 April 2024

Published: 24 April 2024



Copyright: © 2024 by the author. Licensee MDPI, Basel, Switzerland. This article is an open access article distributed under the terms and conditions of the Creative Commons Attribution (CC BY) license (<https://creativecommons.org/licenses/by/4.0/>).

1. Introduction

When two or more adjacent droplets merge on a superhydrophobic surface, spontaneous droplet removal can be induced. This droplet jumping phenomenon was reported by Kollera and Griggull in 1969 during experiments with mercury droplets and was examined by Boreyko and Chen in 2009, observing the jumping phenomenon in droplet coalescence [1]. Coalesced droplet jumping has garnered significant attention in various industrial fields, such as self-cleaning [2,3], anti-icing/frosting [4,5], and enhancement of condensation heat transfer [6,7]. Many researchers have investigated the mechanism and applicability of droplet jumping, developing applied technologies by introducing various factors such as droplet–solid interactions and various surface structures [8].

Superhydrophobic surfaces can rapidly detach when colliding droplets, similar to lotus leaves [9,10]. This surface was able to promote the spontaneous removal of droplets by maintaining the contact angle between droplet and solid at over 150° and keeping the contact angle hysteresis very small. Numerous experiments and theoretical studies have been conducted on the microstructure of superhydrophobic surfaces, and research on improving superhydrophobic surface structures continues. The performance of superhydrophobic surfaces is expressed by the very high contact angle or residence time of droplets, where the residence time can be approximated by $\tau \sim (\rho D^3 / 8\sigma)^{1/2}$ under inviscid fluid conditions [11], where ρ , D , and σ correspond to density, equivalent diameter, and surface tension, respectively. For small droplets, behavior is dominated by inertia force and surface tension. Important dimensionless numbers to express this are the Weber number (We) and

the Reynolds number (Re): the Weber number, $We = \rho DV^2 / \sigma$, represents the inertia force relative to the surface tension, whereas the Reynolds number, $Re = \rho DV / \mu$, represents the inertia force relative to the viscous force, where V is velocity and μ is the viscosity of the liquid.

A few research studies on droplet coalescence jumping have been investigated from various aspects, such as jumping speed and direction, as well as energy conversion. On a flat surface without introduced structures, the jumping speed when two droplets merge is roughly proportional to the inertia-capillary speed of $[\sigma/(\rho D)]^{1/2}$ [12]. Regarding energy conversion, when two droplets combine, surface energy is converted into kinetic energy as part of the motion, inducing a vertical component of velocity on the substrate. On flat surfaces, the jumping speed of droplets can only be limited to a certain maximum, so introducing structures on the surface to increase the energy conversion rate has been proposed [13–18]. Wang et al. [13] introduced triangular prisms to increase jumping speed and reported a high energy conversion rate. Yuan et al. [14] verified an increase in rebound speed and energy conversion rate by introducing an egg-tray structure. Vahabi et al. [15] investigated the energy conversion mechanism by observing internal flow during droplet coalescence. Peng et al. [16] and Liu et al. [17] investigated jumping speed and energy conversion by introducing micro-grooves and U-shaped grooves, respectively, and discussed the horizontal component of jumping direction. Gao et al. [18] proposed asymmetric ridge structures to investigate horizontal movement of droplets on superhydrophobic surfaces and validated the hypothesis through experiments and simulations.

On a horizontal superhydrophobic surface, the dynamics of droplet coalescence-jumping exhibit variations in velocity and droplet morphology, depending on factors such as surface properties, structures, and temperature. Despite these differences, the fundamentals of coalesced droplet jumping remain similar, as follows. Droplets in close proximity form a small liquid bridge. The merging of the droplets is induced by the capillary pressure, along with pressure differences across the interface, which causes droplets to expand. The liquid bridge can induce a vertical upward force near the top of the ridge. The merged droplet exhibits an upward motion, which initiates oscillations. The retraction of the merged droplet begins, and the contact area between the droplet and the substrate surface progressively diminishes. The merged droplet ascends into the air while oscillating horizontally in both directions.

The rebound direction of combined multiple droplets still predominantly remains perpendicular to the plane [12]. When droplets re-approach the surface, they can be removed again due to collisions with other droplets, but horizontal movement can still be restricted [19,20]. The process of droplets re-approaching the surface is very similar to the process of colliding with the surface at low collision speeds. Structures such as point-like defects [21,22] and tapered post arrays [23] have had a significant impact on droplet collision dynamics. It has been reported that adjusting surface wettability during droplet collision can increase the horizontal displacement distance by several tens of times the droplet size [24,25]. However, most studies have implemented changes in the micro/nanostructures of flat surfaces to achieve asymmetric wettability, without considering the influence of wettability on droplet behavior on macro-structures. Furthermore, the durability of micro/nanostructures and surface coatings on macro-structures to maintain superhydrophobicity under practical conditions (such as extreme temperatures) imposes limitations on anti-icing performance. This would lead to asymmetric wettability phenomena on macro-structures and potentially cause defects in vertical jumping performance. Therefore, it is essential to investigate the influence of macro-structure wettability on the horizontal movement of droplets.

This study analyzed numerically the influence of ridge's wettability distribution on droplet coalescence jumping performance using the volume of fluid (VOF) method [26]. As shown in Figure 1, spontaneous merging of two droplets is induced, and due to the presence of superhydrophobic ridges, the droplets completely detach from the surface and recoil. The dynamics of droplet recoil were investigated based on the initial contact angle

ratio ($\beta = \theta_R/\theta_L$) and aspect ratio (AR) of the ridges. Changes in these two factors were examined with respect to the height of the jumping, the horizontal offset distance, and behavioral characteristics, based on the average speed of jumping droplets along each axis. The role of ridge’s wettability distribution and geometric aspect ratio in efficient droplet transportation was analyzed. This study can provide strategies for controlling the direction of droplet jumping and increasing the coalescence frequently between adjacent droplets in related applications.

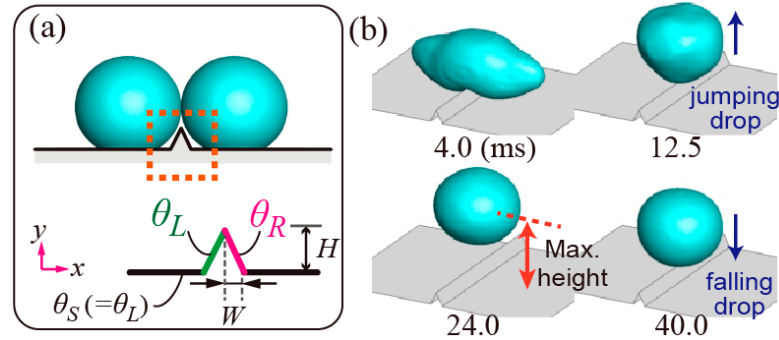


Figure 1. (a) Schematics of droplet coalescence and droplet jumping on a ridged surface with different apparent contact angles of θ_L and θ_R . The wettability of the flat surface is represented as the contact angle of $\theta_S (= \theta_L = 160^\circ)$. The ratio of wettability is defined as $\beta = \theta_R/\theta_L$ in the current study. (b) Shape evolution in the coalescence process. The single droplet has a diameter of the droplet D , and the aspect ratio of the ridge is denoted by a ratio between the height and width (i.e., $AR = H/W$).

2. Numerical Methods

This study analyzed the effect of asymmetry in ridge wettability on droplet coalescence jumping using the VOF numerical analysis method. The behavior of droplet coalescence jumping was investigated by varying the contact angle ratio and the aspect ratio of the ridges. Liquids and gases, namely water and air, were used at room temperature and atmospheric pressure, respectively. The two phases were denoted by subscripts 1 and 2, and the volume fraction was represented by ψ . Numerical analysis was conducted based on previous studies that modeled collision phenomena on solid surfaces [27,28]. The three-dimensional unsteady mass and momentum equations were employed in the computational domain,

$$\frac{\partial}{\partial t}(\rho) + \nabla \cdot (\rho \vec{v}) = 0, \tag{1}$$

$$\frac{\partial}{\partial t}(\rho \vec{v}) + \nabla \cdot (\rho \vec{v} \vec{v}) = -\nabla p + \nabla \cdot [\mu(\nabla \vec{v} + (\nabla \vec{v})^T)] + \rho \vec{g} + 2\sigma\rho\kappa\nabla\psi/(\rho_1 + \rho_2), \tag{2}$$

where $\rho = \psi_2\rho_2 + (1 - \psi_2)\rho_1$, $\mu = \psi_2\mu_2 + (1 - \psi_2)\mu_1$. The curvature of the interface was defined as $\kappa = -(\nabla \cdot \vec{n})$, where \vec{n} is the unit vector normal to the interface, and \vec{g} is the gravitational acceleration. Volume forces were introduced based on a continuous surface tension model [29], and the volume fraction was calculated by employing the equation $\partial\psi/\partial t + \vec{v} \cdot \nabla\psi = 0$, with a surface tracking method based on Rider and Kothe [30]. The discretization model for spatial and temporal derivatives was based on basic convection models and research by Leonard [31], respectively. Residuals were constrained to be less than 10^{-5} to improve convergence of velocity and pressure fields. A time step of 1 μ s and a maximum internal iteration of 25 were applied. A minimum of 50 grid cells were assigned per droplet size to ensure analysis accuracy, and the computational domain introduced a rectangular channel ($10 \times 8 \times 8 \text{ mm}^3$) with ridges on the bottom surface.

In this study, as shown in Figure 1a, the aspect ratio (AR) of the ridge was defined as the ratio of height (H) to width (W), denoted as H/W , with W fixed at 0.2 mm. Three ridge aspect ratios of 1.0, 1.5, and 2.0 were introduced for analysis. Additionally, droplet coalescence jumping on a flat surface without ridges was analyzed to obtain comparative

data. Previous research reported that the advancing and receding contact angles of the droplets were nearly identical at 160° , with negligible contact angle hysteresis [32]. Based on this, static contact angles on the surface (θ_S) and left side (θ_L) were set to 160° to predict jumping behavior. To impart asymmetric contact angles, a static contact angle condition of $\theta_R = 90\text{--}160^\circ$ was applied to the right side. For symmetrical wetting, a relationship of $\beta = \theta_R/\theta_L = 1.0$ (i.e., $\theta_R = 160^\circ$) was satisfied.

The droplet size and properties were defined as $D = 2.0$ mm, $\rho = 998.2$ kg/m³, $\sigma = 0.072$ N/m, and $\mu = 1$ mPa·s, respectively. The diameter of the merged droplet can be calculated using the relationship $D_e = 2^{1/3}D$. The average velocities along each axis were calculated accordingly:

$$U_x^* = \int \rho v_x \psi_2 d\Omega / \int \rho \psi_2 d\Omega, \tag{3}$$

$$U_y^* = \int \rho v_y \psi_2 d\Omega / \int \rho \psi_2 d\Omega, \tag{4}$$

$$U_z^* = \int \rho [v_z \cdot \text{sgn}(z)] \psi_2 d\Omega / \int \rho \psi_2 d\Omega, \tag{5}$$

where v represents velocity components, $\text{sgn}(z)$ is the sign function, and Ω corresponds to volume. Dimensionless mean velocities (U_x, U_y, U_z) were defined by dividing the velocity values obtained from Equations (3)–(5) by the inertia-capillary velocity $[\sigma/(\rho D)]^{1/2}$ [12,18].

To validate the current model, we compared the jumping velocity with the previous theoretical and experimental results on the flat surface without any ridges. The merging of two droplets of the same size on a surface can be characterized by a dimensionless jumping velocity, which follows the inertial-capillary scale of $U_c^* = [\sigma/(\rho R)]^{1/2}$, where R is a radius of the droplet. The relationship between the jumping velocity and inertial-capillary scale can be as follows: $U_y^*/U_c^* = 0.2\text{--}0.3$ [1,12]. Experimental results on the flat surface without any ridges revealed that the relation was $U_y^*/U_c^* = 0.23$, which was made by superhydrophobic nano-coating [18]. Our numerical data with different initial droplet sizes on the surface agreed with the experimental results, as shown in Figure 2.

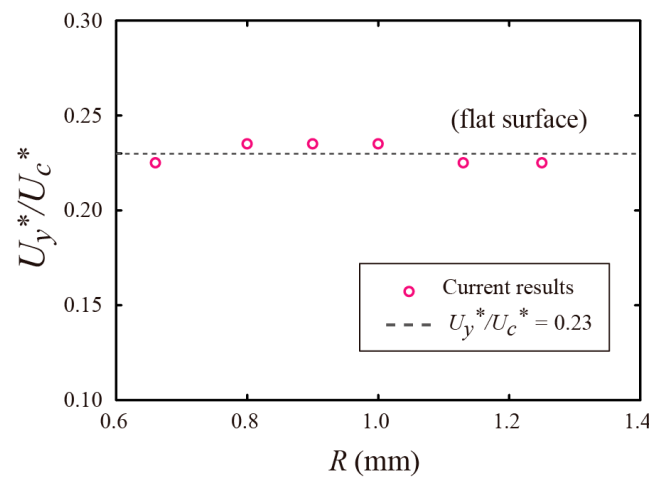


Figure 2. Model validation based on the jumping velocity on the flat surface.

3. Results

To investigate droplet coalescence jumping behavior on ridges with asymmetric wettability, we first predicted the jumping behavior induced by ridges with symmetric wettability. Figure 1b presents the numerical analysis results illustrating the recoil phenomenon due to the surface tension of the merged droplet. A droplet of elliptical shape forms upon coalescence (4.0 ms), and strong recoil forces occur at the ends, where a large curvature is formed, causing the droplet to retract. Due to the presence of hydrophobic ridges, the droplet detaches completely and jumps (12.5 ms). The recoiling droplet reaches its maximum height and falls freely before contacting the ridge again. The assumptions of

this study are as follows: breaking the symmetry of ridge surface wettability leads to the formation of horizontal jumping velocity, and the final landing position of the droplet may vary. This investigation analyzed the dynamics of droplet jumping, focusing on the initial contact angle ratio (β) and the aspect ratio (AR) of the ridges. Variations in these factors were scrutinized concerning the jumping height, horizontal offset distance, and behavioral traits determined by the average speed of jumping droplets along each axis. This study also analyzed the impact of ridge's wettability distribution and geometric aspect ratio on effective droplet transportation.

Predictions of droplet coalescence jumping due to increasing asymmetry in ridge's surface wettability are presented in Figure 3. Figure 3a–c correspond to a geometric aspect ratio (AR) of 1.0, while Figure 3d–f correspond to 2.0. The elliptical shape formed upon droplet fusion was similar in all cases (4.0 ms). During contraction, droplet separation from the surface is slower on ridges with significant wettability asymmetry. Here, the horizontal offset distance is defined as Δx , and its effect becomes more pronounced as β decreases. For instance, at the lowest β , no jumping occurs (Figure 3a), while jumping occurs at slightly higher values of $\beta = 0.66$ and 0.75 (Figure 3b). Upon droplet recontact with the surface, significant differences in droplet volume between the right-hand side (RHS) and left-hand side (LHS) are observed at 30 ms.

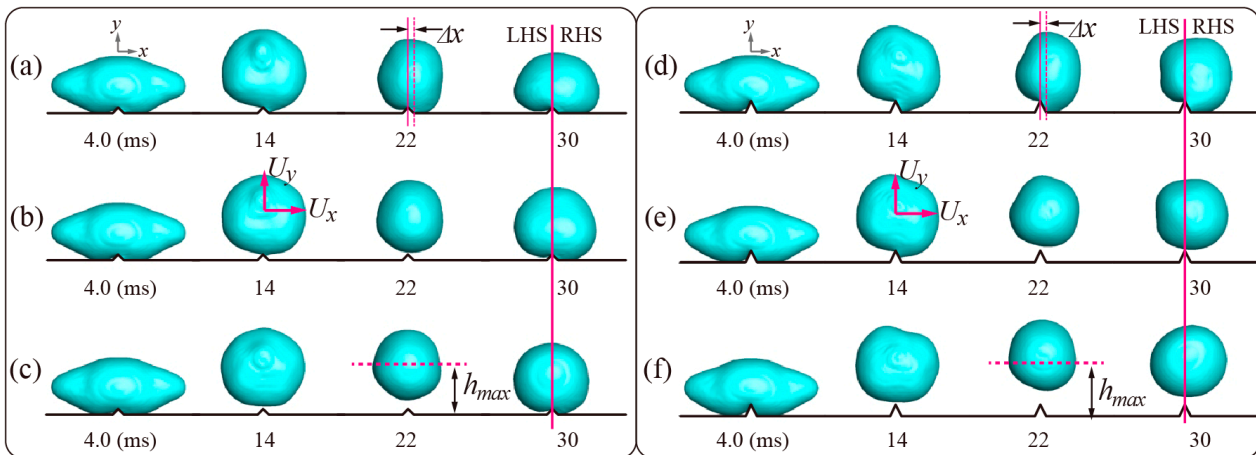


Figure 3. Jumping behavior of the coalesced droplet under two AR s of the ridges. (a–c) Droplet shapes on ridges with (a) $\beta = 0.56$, (b) 0.66 , and (c) 0.75 , under a constant AR of 1.0. (d–f) Droplet shapes on ridges with (a) $\beta = 0.56$, (b) 0.66 , and (c) 0.75 , under a constant AR of 2.0. U_x and U_y represent the averaged jumping velocities of the merged droplets in the x and y directions, respectively. Δx denotes the offset distance of the drop's center from the center of the ridge.

For ridges with high aspect ratios (AR), both the maximum height of the jumping (h_{max}) and the horizontal offset distance (Δx) increase. As seen in Figure 3d–f, during droplet contraction, significant horizontal velocity components are observed at low β , while high recoil results are observed at high β . Additionally, as the ridge's height increases, the vertical velocity component of the droplet also increases. Comparing Figure 3a,d, an increase in ridge height results in a higher horizontal displacement at the same β . Similarly to cases with low aspect ratios, it is observed that the volume of the droplet on the RHS upon recontact with the surface is greater than that on the LHS (Figure 3d at 30 ms).

The effect of asymmetry in wettability on maximum height of the jumping and horizontal offset distance is quantitatively analyzed in Figure 4. The left axis represents the maximum height, while the right axis represents the offset distance, under three ridge's aspect ratios. Generally, as asymmetry increases, the maximum height decreases. For example, compared to symmetric wettability with $\beta = 1.0$ (i.e., $\theta_R = 160^\circ$), the lowest β results in approximately 30% lower height (for $AR = 2.0$). Similarly, for the lowest ridge ($AR = 1.0$), a 21% decrease in height is predicted. Conversely, as asymmetry increases, the offset

distance generally increases. For instance, compared to weak asymmetry, with $\beta = 0.84$ ($\theta_R = 135^\circ$), the lowest β results in an approximately 2.7-fold increase in offset distance (for $AR = 2.0$). Additionally, for the lowest ridge ($AR = 1.0$), an approximately 8-fold increase in height is predicted. Therefore, ensuring uniform wettability distribution on the ridges seems crucial for droplet vertical mobility. When the jumping droplets can be moved again upon re-approaching the surface, due to collisions with solid structures or other droplets, their horizontal movement can occur. The process of droplets re-approaching the surface closely resembles that of collisions with the surface at low speeds. The current prediction of the asymmetric wettability phenomena on macrostructures potentially provides vertical jumping performance in practical applications.

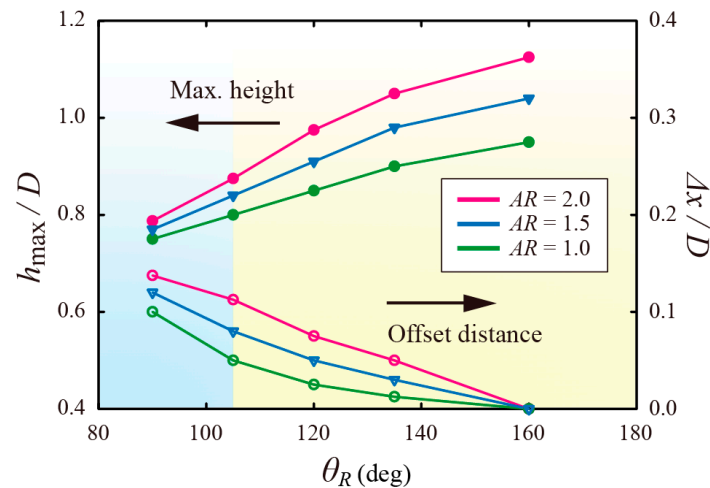


Figure 4. Jumping feature of the coalesced droplet: the maximal height (filled symbol; left axis) and the offset distance (open symbol; right axis), investigated as a function of θ_R , under three AR s of the ridges.

The observed changes in droplet bounce and trajectory variation due to wettability highlight the characteristics of droplet coalescence jumping influenced by wettability. These features can be explained by the horizontal and vertical velocity components of the droplet. Figure 5 depicts the predicted horizontal average velocity (U_x) of the merged droplets over time. For analysis, specific droplet shapes at certain time intervals are included below the graph. Consequently, increased wettability asymmetry induces significant changes in U_x , particularly during contraction, when the droplet detaches from the ridge surface around 10–15 ms. At this moment, a significant difference in U_x is observed due to the disparity in droplet detachment from the left and right sides of the ridge. This difference in detachment maintains a significant disparity in U_x , even after 15 ms. For instance, compared to weak asymmetry with $\beta = 0.84$, a 7.2-fold and a 4.5-fold increase in U_x are predicted at $\beta = 0.56$ and 0.66 , respectively. Moreover, the maximum U_x is predicted around 20–25 ms, coinciding with the maximum height of the jumping. These results suggest that adjusting the distribution of ridge wettability is necessary to control the horizontal velocity of detaching droplets.

The vertical velocity component is crucial in droplet coalescence jumping, as it directly influences self-cleaning and heat transfer performance [12]. Figure 6 shows the temporal variation and maximum values of U_y under wettability asymmetry and the ridge's aspect ratio. Figure 6a,b represent the flat surface without ridges using dashed lines and a star symbol, respectively. From the start of droplet coalescence at 0 s, U_y gradually increases. During the contraction phase, where the droplet shape transitions from elliptical to contracted, U_y sharply increases (5–10 ms). The maximum value of U_y is reached fastest on surfaces without ridges, and next fastest at the lowest β . As the wettability ratio increases, the time taken to reach the maximum vertical velocity increases. U_y starts decreasing around 10–15 ms, when the droplet detaches from the ridge surface. The rate of decrease

in U_y (i.e., the slope of the graph) is highest on surfaces without ridges and next highest at the lowest β . As the difference between θ_R and θ_L decreases, the rate of decrease in U_y relatively diminishes. After approximately 15 ms, the droplet recontacts the ridge, and the velocity approaches zero.

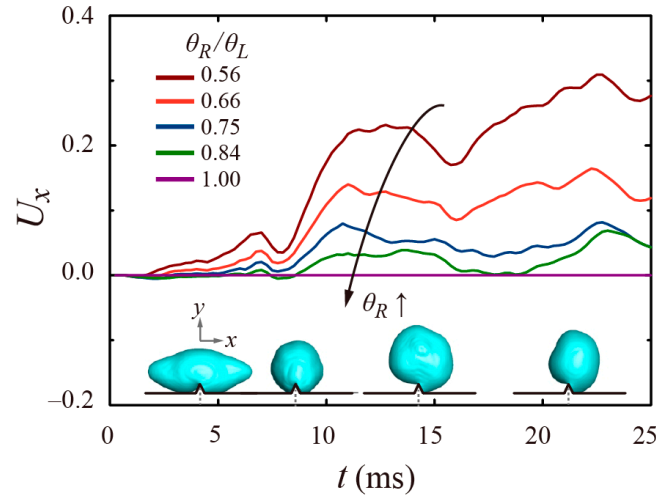


Figure 5. Temporal evolution of averaged jumping velocities of the merged droplets in the x direction for varying β . The snapshots of the inset represent the morphological behavior of the coalesced droplet at several times.

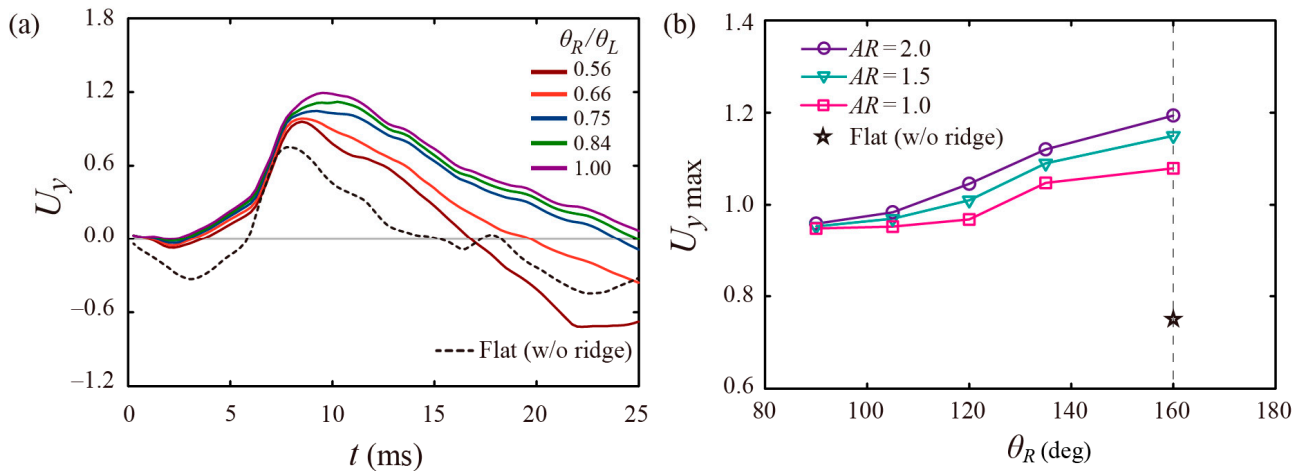


Figure 6. (a) Temporal evolution of averaged jumping velocities of the merged droplets in the y direction for varying β . (b) Maximal U_y as a function of θ_R .

As seen in Figure 6a, the maximum value of U_y decreases as wettability asymmetry increases. This is evident in the graph depicted in Figure 6b, where the maximum value of U_y sharply increases from $\beta = 0.75$ (i.e., $\theta_R = 120^\circ$). In summary, when β is less than 0.75, it can be classified as a region where the influence of ridge wettability difference on jumping is significant (wettability-dependent regime), whereas the opposite is a region for β greater than 0.75, where the influence of ridge wettability difference is less significant (wettability-independent regime). The magnitude of the vertical velocity was predicted under the changes in the ridge’s aspect ratio. For $AR = 1.0, 1.5,$ and 2.0 , the maximum values of U_y were approximately 1.4, 1.5, and 1.6 times greater, respectively, compared to surfaces without ridges. Furthermore, for low β , there was little difference in the maximum values of U_y based on AR , but there was a difference for high β . For example, at $\beta = 0.66$ (i.e., $\theta_R = 105^\circ$), the maximum value of U_y showed a maximum difference of 1.03 times, while the maximum difference in U_y was 1.1 times at $\beta = 1.0$ (i.e., $\theta_R = 160^\circ$). From Figure 6b,

it can be inferred that even if uniform hydrophobicity cannot be maintained due to surface damage, designing for efficient jumping could be achieved by ensuring a large AR .

Investigating the spreading phenomenon when droplets recontact the ridges after jumping may aid in analyzing the final trajectory of the droplets. Figure 7 shows the spreading velocity in the z -direction of the droplet over time. Two cases of droplet shape change for two β values are added above and below the graph. Regardless of β , the variation (period) in the z -directional average velocity up to about 20 ms remained almost the same. However, after the droplet starts spreading on the ridges, around 20 ms, U_z becomes dependent on the initial value of β . For example, at the lowest β (i.e., $\theta_R = 90^\circ$), a long spreading length occurred due to the low receding angle on the ridge (26–36 ms). In contrast, with intermediate values of β , a shorter spreading length occurs due to the high receding angle (26–36 ms). Thus, for β values greater than or equal to 0.75 (i.e., $\theta_R = 120^\circ$), the similar variations of U_z are observed. In summary, when β is less than 0.75, it can be classified as a region where the influence of ridge wettability difference on jumping is significant, whereas the opposite is true for regions with β greater than 0.75, where the influence of ridge wettability difference is less significant, as discussed earlier.

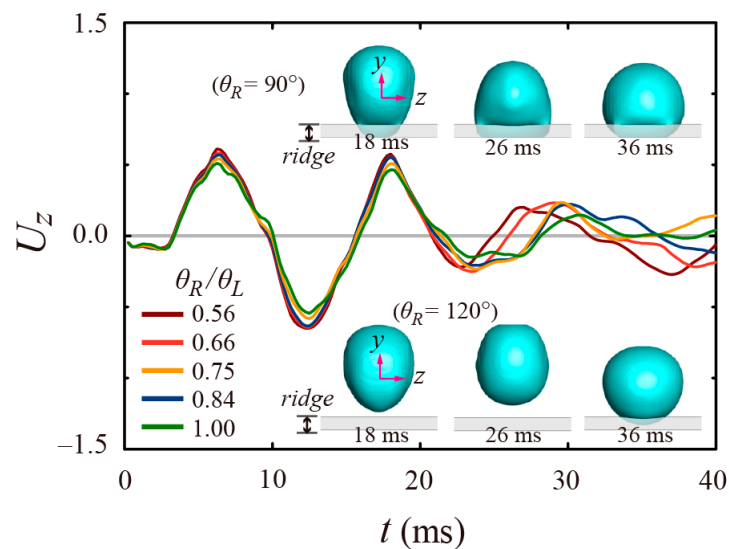


Figure 7. Temporal evolution of averaged jumping velocities of the merged droplets in the z direction for varying β . The snapshots of the insets represent the morphological behavior of the coalesced droplet in the yz plane at three distinct times.

4. Conclusions

Previous research into controlling droplet jumping through macrostructures has primarily emphasized the coalescence stage, with less exploration into how macrostructures affect the motion of a descending jumping droplet. Moreover, many studies focused mainly on the theoretical jumping direction perpendicular to the substrate, although the velocity in the horizontal direction must be involved in practical applications due to various scenarios. This study analyzed numerically the effect of the distribution in ridge structure's wettability on the performance of coalesced droplet jumping. The jumping dynamics were discussed for varying contact angle ratios and the aspect ratios of the ridge, which were the initial values for the current model. The influence of the ridge's wettability asymmetry on droplet coalescence jumping was numerically analyzed. In the current study, while varying the contact angle ratio and the geometric aspect ratio of the ridges, the maximum height of the jumping and horizontal offset distance were predicted. The results showed that at the lowest β , there was approximately a 30% decrease in the height compared to the case with homogenous symmetric wettability. Furthermore, at the lowest β , there was an approximately 2.7-fold increase in the offset distance compared to the case with weak

asymmetry ($\beta = 0.84$). Ensuring uniform wettability of the ridges seems to play a crucial role in efficient droplet transport.

Changes in bounce magnitude and the trajectory of the droplet could be explained by the components of the horizontal and vertical average velocities. Particularly, significant velocity changes occurred around 10–15 ms, when droplets detached from the ridge surface during contraction. This change stemmed from the significantly higher receding velocity on ridges with low wettability surfaces compared to those with high wettability surfaces. As ridge wettability asymmetry increased, the maximum vertical velocity generally decreased. In this study, substantial variations in U_y were observed from $\beta = 0.75$ (i.e., $\theta_R = 120^\circ$). Here, we could classify the region where the influence of surface wettability difference on jumping is significant (wettability-dependent regime) for β values lower than 0.75, and the other region, where the influence of surface wettability difference was less significant (wettability-independent regime), for β values greater than 0.75. This study is expected to contribute to efficient droplet rebound control in applications such as anti-icing/frosting [4,5], enhanced heat transfer [6,7], and energy harvesting [33].

Future studies will involve examining the primary hurdle in the practical implementation of droplet coalescence jumping. Typical superhydrophobic structures face challenges related to mechanical durability and chemical stability, particularly concerning their micro/nanostructures. In addition, practical applications may require further exploration of droplet coalescence jumping across various droplet sizes by using measurements [34]. Lastly, the introduction of multiple droplets brings about greater diversity in their arrangement and characteristics, resulting in a more intricate process and phenomena of coalescence jumping. The multiple droplet coalescence jumping may have a significant influence on the jumping dynamics of the merged droplet.

Funding: This work was supported by the National Research Foundation of Korea (NRF) grant, funded by the Korean government (MSIT) (No. 2022R1C1C1003711).

Institutional Review Board Statement: Not applicable.

Informed Consent Statement: Not applicable.

Data Availability Statement: The raw data supporting the conclusions of this article will be made available by the authors on request.

Conflicts of Interest: The author declares no conflicts of interest.

References

1. Boreyko, J.B.; Chen, C.H. Self-propelled dropwise condensate on superhydrophobic surfaces. *Phys. Rev. Lett.* **2009**, *103*, 184501. [[CrossRef](#)] [[PubMed](#)]
2. Watson, G.S.; Schwarzkopf, L.; Cribb, B.W.; Myhra, S.; Gellender, M.; Watson, J.A. Removal mechanisms of dew via self-propulsion off the gecko skin. *J. R. Soc. Interface* **2015**, *12*, 20141396. [[CrossRef](#)] [[PubMed](#)]
3. Dalawai, S.P.; Aly, M.A.S.; Latthe, S.S.; Xing, R.; Sutar, R.S.; Nagappan, S.; Ha, C.-S.; Sadasivuni, K.K.; Liu, S. Recent advances in durability of superhydrophobic self-cleaning technology: A critical review. *Prog. Org. Coat.* **2020**, *138*, 105381. [[CrossRef](#)]
4. Zhang, Q.; He, M.; Chen, J.; Wang, J.; Song, Y.; Jiang, L. Anti-icing surfaces based on enhanced self-propelled jumping of condensed water microdroplets. *Chem. Commun.* **2013**, *49*, 4516–4518. [[CrossRef](#)]
5. Gong, X.; Gao, X.; Jiang, L. Recent progress in bionic condensate microdrop self-propelling surfaces. *Adv. Mater.* **2017**, *29*, 1703002. [[CrossRef](#)] [[PubMed](#)]
6. Miljkovic, N.; Enright, R.; Nam, Y.; Lopez, K.; Dou, N.; Sack, J.; Wang, E.N. Jumping-droplet-enhanced condensation on scalable superhydrophobic nanostructured surfaces. *Nano Lett.* **2013**, *13*, 179–187. [[CrossRef](#)] [[PubMed](#)]
7. Wen, R.; Li, Q.; Wu, J.; Wu, G.; Wang, W.; Chen, Y.; Ma, X.; Zhao, D.; Yang, R. Hydrophobic copper nanowires for enhancing condensation heat transfer. *Nano Energy* **2017**, *33*, 177–183. [[CrossRef](#)]
8. Liu, C.; Zhao, M.; Zheng, Y.; Cheng, L.; Zhang, J.; Tee, C.A.T. Coalescence-induced droplet jumping. *Langmuir* **2021**, *37*, 983–1000. [[CrossRef](#)]
9. Marmur, A. The lotus effect: Superhydrophobicity and metastability. *Langmuir* **2004**, *20*, 3517–3519. [[CrossRef](#)]
10. Lu, Y.; Sathasivam, S.; Song, J.; Crick, C.R.; Carmalt, C.J.; Parkin, I.P. Robust self-cleaning surfaces that function when exposed to either air or oil. *Science* **2015**, *347*, 1132–1135. [[CrossRef](#)]
11. Clanet, C.; Béguin, C.; Richard, D.; Quéré, D. Maximal deformation of an impacting drop. *J. Fluid Mech.* **2004**, *517*, 199–208. [[CrossRef](#)]

12. Enright, R.; Miljkovic, N.; Sprittles, J.; Nolan, K.; Mitchell, R.; Wang, E.N. How coalescing droplets jump. *ACS Nano* **2014**, *8*, 10352–10362. [[CrossRef](#)] [[PubMed](#)]
13. Wang, K.; Liang, Q.; Jiang, R.; Zheng, Y.; Lan, Z.; Ma, X. Self-enhancement of droplet jumping velocity: The interaction of liquid bridge and surface texture. *RSC Adv.* **2016**, *6*, 99314–99321. [[CrossRef](#)]
14. Yuan, Z.; Gao, S.; Hu, Z.; Dai, L.; Hou, H.; Chu, F.; Wu, X. Ultimate jumping of coalesced droplets on superhydrophobic surfaces. *J. Colloid Interface Sci.* **2021**, *587*, 429–436. [[CrossRef](#)] [[PubMed](#)]
15. Vahabi, H.; Wang, W.; Mabry, J.M.; Kota, A.K. Coalescence-induced jumping of droplets on superomniphobic surfaces with macrotexture. *Sci. Adv.* **2018**, *4*, eaau3488. [[CrossRef](#)] [[PubMed](#)]
16. Peng, Q.; Yan, X.; Li, J.; Li, L.; Cha, H.; Ding, Y.; Dang, C.; Jia, L.; Miljkovic, N. Breaking droplet jumping energy conversion limits with superhydrophobic microgrooves. *Langmuir* **2020**, *36*, 9510–9522. [[CrossRef](#)] [[PubMed](#)]
17. Liu, C.; Zhao, M.; Zheng, Y.; Lu, D.; Song, L. Enhancement and guidance of coalescence-induced jumping of droplets on superhydrophobic surfaces with a U-groove. *ACS Appl. Mater. Interfaces* **2021**, *13*, 32542–32554. [[CrossRef](#)] [[PubMed](#)]
18. Gao, S.; Hu, Z.; Wu, X. Enhanced horizontal mobility of a coalesced jumping droplet on superhydrophobic surfaces with an asymmetric ridge. *Phys. Fluids* **2022**, *34*, 122104. [[CrossRef](#)]
19. Li, T.; Li, M.; Li, H. Impact-induced removal of a deposited droplet: Implications for self-cleaning properties. *J. Phys. Chem. Lett.* **2020**, *11*, 6396–6403. [[CrossRef](#)]
20. Cheng, Y.; Li, J.; Xu, J.; Shen, Y. Numerical investigations of head-on collisions of binary unequal-sized droplets on superhydrophobic walls. *Phys. Fluids* **2021**, *33*, 032001. [[CrossRef](#)]
21. Chantelot, P.; Moqaddam, A.M.; Gauthier, A.; Chikatamarla, S.S.; Clanet, C.; Karlin, I.V.; Quéré, D. Water ring-bouncing on repellent singularities. *Soft Matter* **2018**, *14*, 2227–2233. [[CrossRef](#)] [[PubMed](#)]
22. Jung, H.J.; Yun, S. Splitting behavior of Janus drop impact on protrusion structure. *Phys. Fluids* **2023**, *35*, 062105. [[CrossRef](#)]
23. Hao, C.; Liu, Y.; Chen, X.; Li, J.; Zhang, M.; Zhao, Y.; Wang, Z. Bioinspired interfacial materials with enhanced drop mobility: From fundamentals to multifunctional applications. *Small* **2016**, *12*, 1825–1839. [[CrossRef](#)]
24. Schutzius, T.M.; Graeber, G.; Elsharkawy, M.; Oreluk, J.; Megaridis, C.M. Morphing and vectoring impacting droplets by means of wettability-engineered surfaces. *Sci. Rep.* **2014**, *4*, 7029. [[CrossRef](#)] [[PubMed](#)]
25. Zhao, Z.; Li, H.; Hu, X.; Li, A.; Cai, Z.; Huang, Z.; Su, M.; Li, F.; Li, M.; Song, Y. Steerable droplet bouncing for precise materials transportation. *Adv. Mater. Interfaces* **2019**, *6*, 1901033. [[CrossRef](#)]
26. Hirt, C.W.; Nichols, B.D. Volume of fluid (VOF) method for the dynamics of free boundaries. *J. Comput. Phys.* **1981**, *39*, 201–225. [[CrossRef](#)]
27. Lunkad, S.F.; Buwa, V.V.; Nigam, K.D.P. Numerical simulations of drop impact and spreading on horizontal and inclined surfaces. *Chem. Eng. Sci.* **2007**, *62*, 7214–7224. [[CrossRef](#)]
28. Yun, S.; Lim, G. Ellipsoidal drop impact on a solid surface for rebound suppression. *J. Fluid Mech.* **2014**, *752*, 266–281. [[CrossRef](#)]
29. Brackbill, J.U.; Kothe, D.B.; Zemach, C. A continuum method for modeling surface tension. *J. Comput. Phys.* **1992**, *100*, 335–354. [[CrossRef](#)]
30. Rider, W.J.; Kothe, D.B. Reconstructing volume tracking. *J. Comput. Phys.* **1998**, *141*, 112–152. [[CrossRef](#)]
31. Leonard, B.P. A stable and accurate convective modeling procedure based on quadratic upstream interpolation. *Comput. Methods Appl. Mech. Eng.* **1979**, *19*, 59–98. [[CrossRef](#)]
32. Abolghasemibizaki, M.; Dilmaghani, N.; Mohammadi, R.; Castano, C.E. Viscous droplet impact on nonwetttable textured surfaces. *Langmuir* **2019**, *35*, 10752–10761. [[CrossRef](#)] [[PubMed](#)]
33. Khatir, Z.; Kubiak, K.J.; Jimack, P.K.; Mathia, T.G. Dropwise condensation heat transfer process optimisation on superhydrophobic surfaces using a multi-disciplinary approach. *Appl. Therm. Eng.* **2016**, *106*, 1337–1344. [[CrossRef](#)]
34. Mouterde, T.; Nguyen, T.-V.; Takahashi, H.; Clanet, C.; Shimoyama, I.; Quéré, D. How merging droplets jump off a superhydrophobic surface: Measurements and model. *Phys. Rev. Fluids* **2017**, *2*, 112001. [[CrossRef](#)]

Disclaimer/Publisher’s Note: The statements, opinions and data contained in all publications are solely those of the individual author(s) and contributor(s) and not of MDPI and/or the editor(s). MDPI and/or the editor(s) disclaim responsibility for any injury to people or property resulting from any ideas, methods, instructions or products referred to in the content.